Scaling law for bubbles induced by different external sources: Theoretical and experimental study

S. W. Gong, S. W. Ohl, and E. Klaseboer
Institute of High Performance Computing, 1 Fusionopolis Way, No. #16-16, Connexis, Singapore 138632, Singapore

B. C. Khoo
Department of Mechanical Engineering, National University of Singapore, 10 Kent Ridge Crescent, Singapore 119260, Singapore
(Received 11 March 2009; revised manuscript received 17 February 2010; published 20 May 2010)

The scaling relations for bubbles induced by different external sources are investigated based on a modified Rayleigh model and experimental observations. The equations derived from the modified Rayleigh model are presented to describe the collapse of bubbles induced by the different external sources such as electrical spark, laser, and underwater explosion. A scaling law is then formulated to establish the scaling relations between the different types of bubbles. The scaling law reveals the fact that the characteristic length scale factor differs from the characteristic time scale factor for the different types of bubbles. It is then validated by our experimental observations of the spark- and laser-generated bubbles as well as the bubbles induced by underwater explosions from previous published reports. With the present scaling law, studies on spark- or laser-generated bubbles as well as their applications (for example, in industrial or biomedical related applications) can benefit from the experiences and information built up over the years in underwater explosion bubbles. Conversely, it is possible to substitute a spark- or laser-generated bubble for an underwater explosion bubble in the study of a large-scale and complex physical problem.

DOI: 10.1103/PhysRevE.81.056317 PACS number(s): 47.55.dd, 47.55.dp

I. INTRODUCTION

Bubble dynamics has been studied extensively for many decades. Early work focused on the bubbles induced by underwater explosions [1]. Since the 1960s, spark and laser techniques for the generation of bubbles have been developed [2,3]. In recent years, there is a resurgence of interest in underwater explosion bubbles [4] as well as bubbles induced by sparks [5–10] and lasers [11–19]. This growing interest is driven by the bubbles' increasing applications in marine, industrial, and biomedical research [20–35].

The bubbles induced by underwater explosions have been well explored by Cole [1]. For a free field explosion, the maximum bubble radius and the bubble period can be determined using empirical equations in terms of explosive charge weight, charge depth, and a parameter based on extensive field testing and observations [1,6,9]. The growth and collapse of a bubble generated by spark or laser are similar in principle to the bubble induced by an underwater explosion, although there are some differences between them. The experimental and numerical results given by Buogo and Cannelli [8] showed that the spark-generated bubble was consistent with the Rayleigh model [36] of a cavity in an incompressible fluid with the assumption of a relatively high vapor pressure. The studies of Petkovšek and Gregorčič [18] showed that the Rayleigh model [36] can be used to describe the expansion and collapse of a laser-generated bubble. It would be favorable to explore if spark- or laser-generated bubbles can (partly) replace underwater explosion bubbles experimentally, because bubble generation with spark and laser has the merits of economy, safety, and environmental conservation with relatively low cost compared to bubble generation involving explosives. On the other hand, research on spark- or laser-generated bubbles, as well as their applications can benefit from the experiences built up over the years in underwater explosion bubbles. For example, cavitation bubbles may form during laser *in situ* keratomileusis (LASIK) surgery, and its dynamics are relevant for the success of the treatment, as well as the extent of undesirable collateral damage sustained by the patient [34]. Also as reported in [35], the cavitation bubble dynamics are very sensitive to the physical properties (the Young's modulus, density, and Poisson ratio) of the nearby biomaterials (bone, cartilage, skin, etc.). The bubbles collapse with a high-speed jet near hard biomaterials such as bone and cartilage, but split into smaller bubbles which form opposite jets as they collapse near other biomaterials such as muscle. To exploit the advantage of the different bubble generation methods, an appropriate scale law is, therefore, necessary to link the bubbles induced by the different external sources such as underwater explosion, electric spark, and laser, taking into account the different physical processes involved in each of these sources. To the authors' best knowledge, however, such a scaling relationship has not been published in the open literature.

In this paper, we will establish the scaling relations for the bubbles induced by the different external sources, in particular for the bubbles induced by underwater explosion, electrical spark, and laser. The modified Rayleigh model is used including the effects from the small density change of the surrounding fluid, the pressure inside the bubble, and the water depth at the inception point of the bubble. Based on the modified Rayleigh model, an equation for the bubble wall velocity is derived. The solution to the nondimensionalized equation for the bubble wall velocity leads to the explicit evaluation of the bubble collapse time (i.e., the modified Rayleigh collapse time) which enables the charac-

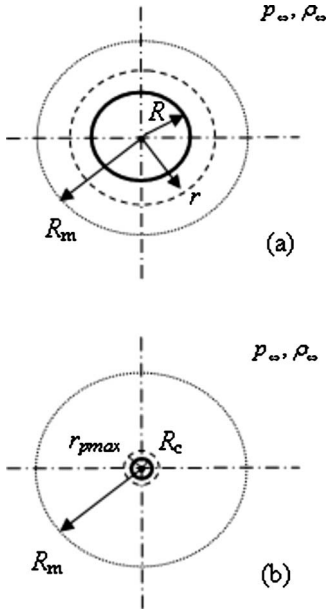

FIG. 1. Schematic description of the modified Rayleigh model. (a) Bubble contracting from R_m to R at time t. (b) At the final collapse, bubble radius R_c tends toward zero ($R_c \to 0$ when $t \to t_c$); the maximum pressure p_{max} occurs at $r=r_{p\,max}$ ($r_{p\,max} > R_c$).

terization of the different bubbles on the same theoretical basis. We then, in terms of the modified Rayleigh collapse time, propose the scaling law that elaborates on the scaling relations between different bubbles such as the spark- or laser-generated bubbles and underwater explosion bubbles. We also demonstrate that the results of the present scaling law are consistent with the experimental results.

II. THEORETICAL INVESTIGATIONS

A. Modified Rayleigh model

The Rayleigh model [36] describes an empty spherical bubble (or cavity) contracting and collapsing from a maximum radius R_m to a minimum radius R_c ($R_c \to 0$) in an ideal incompressible liquid with a constant density ρ_∞. Using an energy-balance approach, elegant solutions were obtained [36] for the bubble wall velocity, $dR/dt = \sqrt{(2p_0/3\rho_\infty)(R_m^3/R-1)}$, and the bubble collapse time, $t_c \approx 0.915\sqrt{p_\infty/p_0}R_m$. A constant hydrostatic pressure p_0 at any point of the fluid was assumed. In the current study, we use a modified Rayleigh model to study the bubble collapse. The modified Rayleigh model takes into account the effects of the pressure inside the bubble, the water depth at the inception point of the bubble, and the compressibility of the fluid surrounding the bubble wall during the bubble collapse. These effects are, in general, influenced by the different external sources or means of bubble generation.

The schematic description of the modified Rayleigh model for bubble collapsing from R_m to R_c is shown in Fig. 1, in which ρ_∞ and p_∞ denote the density and the pressure in the undisturbed fluid, respectively. When the bubble collapses ($t \to t_c$), the bubble radius tends toward zero ($R_c \to 0$) and the maximum pressure p_{max} occurs at a distance $r_{p\,max}$ from the bubble center. The density of the fluid surrounding the bubble wall can be expressed as $\rho=\rho_\infty+(\rho-\rho_\infty)=\rho_\infty(1+\Delta\rho/\rho_\infty)$. The small density change $\Delta\rho=\rho-\rho_\infty$ here actually reflects the influence of the compressibility of the fluid surrounding the bubble wall. Let $\Delta\rho_c$ denote the small density change of the fluid surrounding the bubble wall at the distance of $r_{p\,max}$. Since both $\Delta\rho_c$ and $\Delta\rho$ are very small in comparison to ρ_∞, this justifies the assumption that $\Delta\rho/\rho_\infty \approx \Delta\rho_c/\rho_\infty$, and thus the density of the fluid surrounding the bubble wall can be approximated as $\rho \approx \rho_\infty(1+\Delta\rho_c/\rho_\infty)$.

Consider the bubble wall contracting from its maximum radius R_m to R at time t; the kinetic energy of the whole fluid can be estimated by

$$E_{kin} = \frac{1}{2}\int_V \rho_\infty\left(1+\frac{\Delta\rho_c}{\rho_\infty}\right)\left(\frac{dr}{dt}\right)^2 dV = \frac{1}{2}\int_S \rho_\infty R\left(1+\frac{\Delta\rho_c}{\rho_\infty}\right)\left(\frac{dR}{dt}\right)^2 dS = 2\pi\rho_\infty\left(1+\frac{\Delta\rho_c}{\rho_\infty}\right)\left(\frac{dR}{dt}\right)^2 R^3, \quad (1)$$

where the Gauss theorem is used to convert the integral over the whole fluid domain V into a surface integral over the bubble surface S [30,37]; dR/dt is the bubble wall velocity and dr/dt is the simultaneous velocity at any distance r (greater than R) from the center. The work done from the initial radius R_m to R is

$$\frac{4}{3}\pi p_m(R_m^3 - R^3) = \frac{4}{3}\pi p_m\left(\frac{R_m^3}{R^3}-1\right)R^3, \quad (2)$$

where p_m is a constant pressure over the collapse phase period. Following Rayleigh's energy-balance approach [36] with equating Eqs. (1) and (2), we have

$$\left(1+\frac{\Delta\rho_c}{\rho_\infty}\right)^{1/2}\frac{dR}{dt} = -\left[\frac{2p_m}{3\rho_\infty}\left(\frac{R_m^3}{R^3}-1\right)\right]^{1/2}. \quad (3)$$

When $\Delta\rho_c$ is very small compared to ρ_∞, we may write

$$\left(1+\frac{\Delta\rho_c}{\rho_\infty}\right)^{1/2} = \left[1+\frac{1}{2}\frac{\Delta\rho_c}{\rho_\infty}-\frac{1}{2}\frac{1}{4}\left(\frac{\Delta\rho_c}{\rho_\infty}\right)^2\cdots\right] \approx \left(1+\frac{1}{2}\frac{\Delta\rho_c}{\rho_\infty}\right), \quad \frac{\Delta\rho_c}{\rho_\infty} \ll 1. \quad (4)$$

Let $\mu_\alpha=(1/2)(\Delta\rho_c/\rho_\infty)$ and $p_m=p_\infty-p_i+\rho_\infty g D_\alpha$, where p_i is the average pressure inside the bubble, D_α is the water depth at the inception of the bubble, g is the acceleration of gravity, and the subscript α denotes an external source for bubble generation and it shall be substituted by the first letter for the specified source of the bubble generation (e.g., u for underwater explosion, s for spark, and L for laser). Substituting Eq. (4) with $\mu_\alpha=(1/2)(\Delta\rho_c/\rho_\infty)$ into Eq. (3), we have the expression for the bubble wall velocity during the collapse in the form of

$$\frac{dR}{dt} = -(1+\mu_\alpha)^{-1}\left[\frac{2(p_\infty - p_i + \rho_\infty g D_\alpha)}{3\rho_\infty}\left(\frac{R_m^3}{R^3} - 1\right)\right]^{1/2}. \tag{5}$$

We define the dimensionless time

$$t' = \frac{t}{(1+\mu_\alpha)R_m\sqrt{\dfrac{\rho_\infty}{(p_\infty - p_i + \rho_\infty g D_\alpha)}}}, \tag{6}$$

and the dimensionless bubble radius

$$R' = \frac{R}{R_m}, \tag{7}$$

and then nondimensionalized Eq. (5) can be written in the concise form of

$$\frac{dR'}{dt'} = -\left(\frac{2}{3}\right)^{1/2}\left(\frac{1}{R'^3} - 1\right)^{1/2}. \tag{8}$$

From Eq. (8), the dimensionless bubble collapse time can be calculated by

$$\begin{aligned} t'|_{t=t_c} &= \frac{t_c}{(1+\mu_\alpha)R_m\sqrt{\dfrac{\rho_\infty}{(p_\infty - p_i + \rho_\infty g D_\alpha)}}} \\ &= -\left(\frac{3}{2}\right)^{1/2}\int_1^0 \frac{R'^{3/2}}{(1-R'^3)^{1/2}}dR' \\ &= 0.915, \end{aligned} \tag{9}$$

and consequently the modified Rayleigh collapse time is obtained in the expression

$$t_c = 0.915(1+\mu_\alpha)R_m\sqrt{\frac{\rho_\infty}{(p_\infty - p_i + \rho_\infty g D_\alpha)}}. \tag{10}$$

The density parameter μ_α in Eq. (10) accommodates the difference between the Rayleigh model and the present modified model as shown in Fig. 2; it depends on the pressure of the fluid surrounding the bubble at the final collapse. By using the equation of state of the modified Tait form [1,38]

$$\frac{p+B}{p_\infty + B} = \left(\frac{\rho}{\rho_\infty}\right)^n, \tag{11}$$

where the values $B=3049.13$ bars and $n=7.15$ give an excellent fit to the experimental pressure-density relation for water up to 10^5 bars [1,38]; the density parameter μ_α in Eq. (10) can be estimated by

$$\mu_\alpha = \frac{\Delta\rho_c}{2\rho_\infty} = \frac{1}{2}\left[\left(\frac{p_{max}+B}{p_\infty + B}\right)^{1/n} - 1\right], \tag{12}$$

where p_{max} is the maximum fluid pressure at a distance $r_{p\,max}$ from the center of the bubble at the final collapse.

By integrating numerically Eq. (5) [or Eq. (8) in conjunction with Eqs. (6) and (7)], the bubble radius as a function of time can be obtained when the bubble is contracting (collapsing) from a maximum radius R_m to a minimum radius R_c ($R_c \to 0$). These equations based on the modified Rayleigh model shown in Fig. 1 provide the basis for comparison and evaluation of the different bubbles induced by different external sources. The modified Rayleigh collapse time [Eq. (10)] will be used to establish the scaling law between the different bubbles.

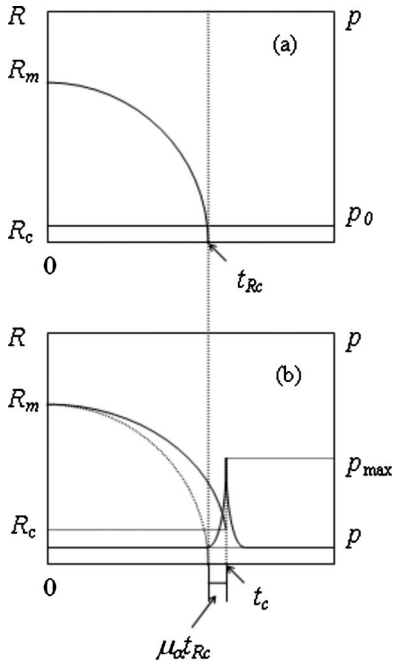

FIG. 2. Schematic description of the density parameter μ_α. (a) For the Rayleigh model. (b) For the modified Rayleigh model. Note that there are basically two differences between the two models: (1) the pressure surrounding the bubble is kept constant at p_0 for the Rayleigh model, while it varies considerably for the modified model during the final collapse; (2) the collapse times differs by a factor $\mu_\alpha t_{Rc}$ between the two models, where t_{Rc} is the Rayleigh collapse time, t_c is the modified Rayleigh collapse time, and μ_α is the density parameter. (Assume $p_m = p_0$ here for the sake of describing μ_α.)

B. Maximum radius R_m and bubble collapse time t_c

The maximum radius R_m is essential for determining the bubble collapse time as shown in Eq. (10). We will explore the maximum radius R_m as well as the bubble collapse time t_c of two typical but different bubbles: one is a large bubble induced in an underwater explosion and the other is a small bubble induced by spark or laser. In an underwater explosion, the potential energy E stored in the water is proportional to the maximum volume V_m of the bubble multiplied by the reference pressure at the charge depth D_u [1,39], which can be expressed as

$$E = \left(\frac{4\pi}{3}\right)(R_m)_u^3(p_\infty - p_i + \rho_\infty g D_u). \tag{13}$$

Using the coefficient K_{EW} to represent the potential energy E per charge weight W (i.e., $K_{EW}=E/W$), we can estimate the maximum explosive bubble radius $(R_m)_u$ (in meters) via

$$(R_m)_u = \left(\frac{3K_{EW}}{4\pi\rho_\infty g}\right)^{1/3} \frac{W^{1/3}}{\left(D_u + \frac{p_\infty - p_i}{\rho_\infty g}\right)^{1/3}}. \tag{14a}$$

The coefficient K_{EW} in $(\mathrm{m/s})^2$ is a measure of energy effectiveness of an explosive charge, which can be obtained from underwater explosive tests for different types of charges. By defining $K_R=(3K_{EW}/4\pi\rho_\infty g)^{1/3}$ with $p_\infty=10^5$ Pa (ambient pressure), $\rho_\infty=1000$ kg/m^3, and $g\approx 10$ m/s^2, and ignoring the internal (vapor) pressure, Eq. (14a) becomes

$$(R_m)_u = K_R \frac{W^{1/3}}{(D_u+10)^{1/3}}, \tag{14b}$$

which is exactly the same as the classic empirical equation that was widely used for the estimation of the maximum radius of an underwater explosion bubble [1,40].

The maximum radii of the spark- and laser-generated bubbles can be measured experimentally. In the spark and laser experiments, the potential energy stored in water is also proportional to the maximum volume of the bubble multiplied by the pressure $p_m=p_\infty-p_i+\rho_\infty g D_\alpha$. The maximum radius of the spark- or laser-generated bubble can then be estimated with the electric energy measured from experiments [8] or with the energy of the breakdown pulse [18] based on Eq. (13) (by substituting the subscript α for subscript u). As such, there could be some degree of consistency between the maximum radii of the spark-generated bubble $(R_m)_s$, laser-generated bubble $(R_m)_L$, and the respective energy input based on Eq. (13). On the other hand, an estimation of $(R_m)_s$ or $(R_m)_L$ in terms of $(R_m)_u$ in Eq. (14) is still possible provided the electrical or laser energy input is expressed in terms of their equivalent W and K_R.

After the maximum bubble radius R_m is evaluated, Eq. (10) can be used to predict the collapse time of the different types of bubbles, such as the spark-generated bubbles, laser-generated bubbles, and underwater explosion bubbles. Furthermore, the collapse time of the underwater explosion bubbles can be estimated in another optional way. From Eqs. (10) and (14a), and neglecting the internal (vapor) pressure, we can express the collapse time of an underwater explosion bubble in the form of

$$(t_c)_u = \frac{0.915(1+\mu_u)}{g^{5/6}} \left(\frac{3K_{EW}}{4\pi\rho_\infty}\right)^{1/3} \frac{W^{1/3}}{\left(D_u + \frac{p_\infty}{\rho_\infty g}\right)^{5/6}}. \tag{15a}$$

When we define $K_T=2[0.915(1+\mu_u)/g^{5/6}](3K_{EW}/4\pi\rho_\infty)^{1/3}$ with $p_\infty=10^5$ Pa, $\rho_\infty=1000$ kg/m^3, we have the collapse time $(t_c)_u$ (or the oscillation period T_u) of the underwater explosion bubble

$$(t_c)_u \approx \frac{T_u}{2} = \frac{K_T}{2} \frac{W^{1/3}}{(D_u+10)^{5/6}}, \tag{15b}$$

which is consistent with the classic empirical equation for the estimation of the oscillation period, $T_u\approx 2(t_c)_u = K_T[W^{1/3}/(D_u+10)^{5/6}]$, for the underwater explosion bubble [1,40].

C. Scaling of bubbles induced by different sources

The dimensionless Eq. (8) shows that the bubbles induced by different external sources can be expressed as a consistent dimensionless bubble. This implies that two different bubbles in their collapse phases can proportionally be related by a characteristic time scale factor λ_T and a characteristic length scale factor λ_R, as long as their collapse times are known.

We shall focus on the above-mentioned two different bubbles, namely, a large bubble induced by an underwater explosion and a small bubble induced by spark or laser. Let t'_u and t'_α denote the dimensionless time instants for an underwater explosion bubble and a bubble induced by spark or laser, respectively (the subscript α can be substituted by s for spark or L for laser accordingly). When both the underwater explosion bubble, and the spark- or laser-generated bubble are nondimensionalized, the R'_u-t'_u curve should coincide with the R'_α-t'_α curve accordingly based on Eq. (8), and thus $t'_u/t'_\alpha=1$ if $R'_u/R'_\alpha=1$. Therefore, the relation between the actual (dimensional) time of the large bubble generated by underwater explosion and the actual (dimensional) time of the small bubble generated by the spark or the laser can be expressed as

$$\lambda_T = \frac{t_u}{t_\alpha} = \frac{(t_c)_u}{(t_c)_\alpha} = \frac{1+\mu_u}{1+\mu_\alpha} \sqrt{\frac{p_\infty - (p_i)_\alpha + \rho_\infty g D_\alpha}{p_\infty - (p_i)_u + \rho_\infty g D_u}} \frac{(R_m)_u}{(R_m)_\alpha}. \tag{16}$$

Next, let R_u and R_α denote the actual (dimensional) radius of an underwater explosion bubble and the actual (dimensional) radius of a bubble induced by spark or laser (the subscript α can be substituted by s for spark or L for laser). The relation of the two different dimensional radii can be expressed by

$$\lambda_R = \frac{R_u(t_u)}{R_\alpha(\lambda_T t_\alpha)} = \frac{(R_m)_u}{(R_m)_\alpha}. \tag{17}$$

Substituting Eq. (17) into Eq. (16), the characteristic time scale factor (16) can be rewritten as

$$\lambda_T = \frac{t_u}{t_\alpha} = \frac{(t_c)_u}{(t_c)_\alpha} = \frac{1+\mu_u}{1+\mu_\alpha} \sqrt{\frac{p_\infty - (p_i)_u + \rho_\infty g D_\alpha}{p_\infty - (p_i)_\alpha + \rho_\infty g D_u}} \lambda_R. \tag{18}$$

Equation (18) shows the difference between the characteristic time scale factor λ_T and the characteristic length scale factor λ_R, i.e., $\lambda_T\neq\lambda_R$, which reflects the difference arising from the different sources for bubble generation. Equation (18) also implies that the ratio of λ_T/λ_R would be a constant if μ_u and μ_α are constants.

Based on Eqs. (17) and (18), the actual (dimensional) radius-time curve of an underwater explosion bubble during the collapse time can be represented by the actual (dimensional) radius-time curve of a spark or laser bubble if the characteristic time and length scale factors λ_T and λ_R are known.

III. EXPERIMENTS

In this study, both the spark-and laser-generated bubbles were measured experimentally. The spark bubble was gener-

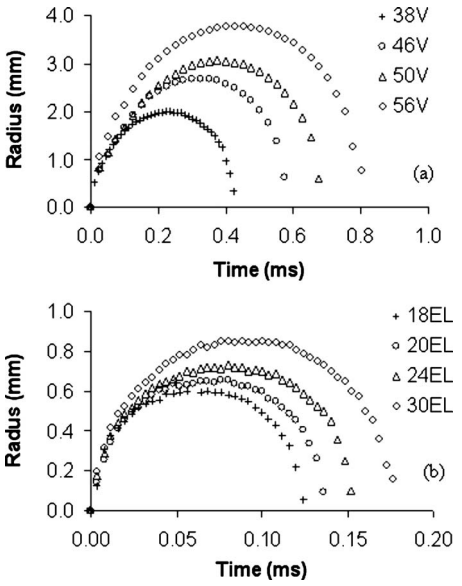

FIG. 3. (a) Measured radius-time curves of the bubbles induced by the spark with different voltages. (b) Measured radius-time curves of the bubbles induced by the laser with different energy levels; here, EL denotes energy level.

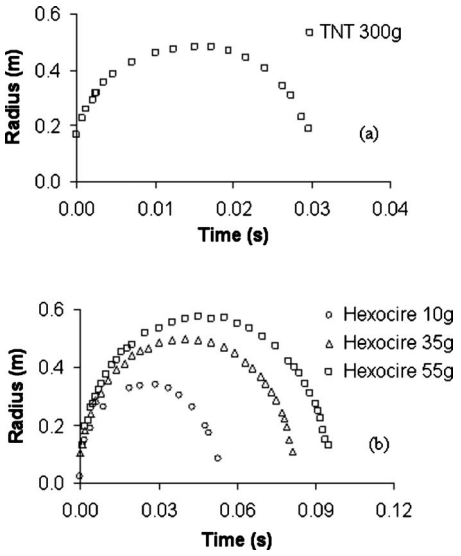

FIG. 4. (a) Measured radius-time curve of the bubble generated by a 300 g TNT explosive at a water depth of 91.5 m [40]. (b) Measured radius-time curves of the bubbles, respectively, generated by Hexocire explosive charges of 10, 35, and 55 g at a water depth of 3.5 m [41].

ated by short circuiting a pair of very thin electrodes (~0.117 mm in diameter) which are connected to a charged capacitor (3300 μF). The capacitor was charged up to a voltage of 57 V via a charging circuit which consists of a current source and a 1 kΩ resistor. Both electrodes were submerged in a water tank of $17\times17\times17$ cm^3 which was filled to about 90% with tap water. The crossing point of the electrodes was placed at about the middle of the tank so as to eliminate the influence of the nearby walls and the free surface on the bubble. The video of the bubble was made using a Photron Fastcam Ultima APX high-speed camera with a filming rate of 40 000 frames per second (fps) (for 46, 50, and 56 V), and 90 000 fps (for 38 V); and a shutter speed of 1/80 000 s (for 46, 50, and 56 V) and 1/120 000 s (for 38 V). The front lighting was provided by a 400 W spotlight.

The laser-induced cavitation bubble was created by using the Orion Nd:YAG laser system from New Wave Research (Fremont, CA). This is a frequency doubled laser which is fitted with a lens system that focuses the laser into a small water tank of $3\times3\times5$ cm^3. The laser energy used was approximately 5 mJ and the laser pulse lasts for about 7 ns. A bubble was generated by the plasma at the point of focus of the laser. The bubble expands rapidly and cools to the liquid temperature a few microseconds later [11]. The bubble dynamics was captured using the Photron SA 1.1 high-speed camera with a filming rate of 250 000 frames per second and a shutter speed of 1/250 000 s.

IV. RESULTS AND DISCUSSIONS

A. Density parameter μ_α

Figures 3 and 4 show the bubbles generated, respectively, by the different external sources: the spark, the laser, and the underwater explosion. We will use these experimental data to justify the present modified Rayleigh model and the density parameter μ_α. The four sets of the spark- and laser-generated bubbles shown in Fig. 3 were measured from the high-speed photographs taken from the above-described experiments. The underwater explosion bubbles shown in Fig. 4 were generated by underwater explosions of two different charges. One of the bubbles was generated by a 300 g trinitrotoluene (TNT) explosive charge detonated at a water depth of 91.5 m; it was reproduced from Swift and Decius' experimental data [40]. The other three bubbles were created by explosive charges of Hexocire (RDX+wax) with weights of 10, 35, and 55 g, respectively, detonated at a depth of 3.5 m, whose curves were reproduced from the coauthors' previous paper [41]. Details of the experiment for the second type of underwater explosion bubbles can also be found in the same paper [41].

Based on the modified Rayleigh model as shown in Fig. 1, the collapse of different bubbles can be simulated via Eq. (8) in conjunction with Eqs. (6) and (7), in which the density parameter μ_α can be estimated with Eq. (12). From Eq. (12), it can be seen that the density parameter μ_α depends on the maximum pressure p_{max}; in other words, the density parameter μ_α can be obtained if the maximum pressure p_{max} is known. The value of the internal pressure p_i, corresponding to the value of μ_α, can be evaluated via Eq. (10) (which can be rewritten in the form of $p_i=(p_\infty+\rho_\infty g D_\alpha)-\rho_\infty[0.915(1+\mu_\alpha)R_m]^2/t_c^2$ in conjunction with the experimental data of the maximum bubble radius R_m and the collapse time t_c).

Using Eq. (12), one can easily find that $\mu_\alpha<0.01$ when $p_{max}<200p_\infty$, which implies that the effect of the density change can be ignored when p_{max} does not exceed $200p_\infty$. For the spark bubble with a relatively high vapor pressure [8], the pressure around the bubble wall can be estimated by [42,43] $p(r)/p_m=1+R'/(3r')(1/R'^3-4)-R'^4/(3r'^4)(1/R'^3-1)$, where $r'=r/R_m$. For $R'=R_c/R_m=0.1$, $r_{p\,max}=1.59R_c$,

TABLE I. The measured data for the spark-generated bubbles; the predicted density parameter μ_s and the internal pressures with $p_\infty=0.1$ MPa, $\rho_\infty=1000$ kg/m^3, and $g=9.81$ m/s^2; V stands for voltage used in spark test.

External source	V	D_s (m)	$(R_m)_s$ (mm)	$(t_c)_s$ (ms)	p_{max} (MPa)	μ_s [Eq. (12)]	P_i [Eq. (10)] (MPa)
Spark	38	0.06	1.99	0.216			
	46	0.06	2.69	0.291			
	50	0.06	3.04	0.330	<20	~ 0	0.03
	56	0.06	3.77	0.410			

$p_{max}=p(r_{pamx})<200p_\infty$, and thus $\mu_s<0.01$. And, therefore, the internal pressure of the spark bubbles, estimated by Eq. (10), tends to 0.03 MPa with $\mu_s\approx 0$ (see Table I), which is consistent with the values used in the previous published references [8,44]. Similarly, the effect of the density change in laser bubble collapsing may be ignored when the maximum pressure p_{max} surrounding the bubble wall induced by the laser is less than $200p_\infty$. The internal pressure of the laser bubbles tends to 0.022 MPa with $\mu_L\approx 0$ (see Table II).

In contrast, the effect of the density change becomes obvious as the maximum pressure increases beyond $O(1000)p_\infty$. For example, when the maximum pressure p_{max} reaches $1500p_\infty$, μ_u exceeds 0.05 (which occurs commonly in the underwater explosion). For a TNT charge, the maximum pressure can be estimated by the empirical equation (in SI unit) [45] $p_{max}=9.4395\times 10^6(W^{1/3}/r_{p\,max})(1-4k^4)$, with $k=0.0742(D_u+10)^{\gamma-1}$, $r_{p\,max}=1.59R_c$, and the ratio of specific heats, $\gamma=1.25$. This equation for the maximum pressure can also be used for the explosive charges of Hexocire based on a TNT equivalent charge [41]. Table III shows the estimation of the density parameter μ_u based on Eq. (12) for the underwater explosion bubbles. With those density parameters μ_u in Table III, the internal pressure of the underwater explosion bubbles can be estimated using Eq. (10); it tends to zero (see Table III), which matches well with the experiment results [40,41].

B. Modified Rayleigh model for bubble collapse

The Rayleigh model [36] describes an empty bubble collapsing from a maximum radius to a minimum radius in an ideal incompressible liquid. In view of its simplicity, the Rayleigh model has preserved its significance that often makes it possible to obtain a better insight into the physical process involved in the bubble collapsing. A great number of works have been done in corroborating and applying Rayleigh's model to analyze real-life bubbles [46–52], which have been well summarized in Refs. [38,42,43]. The Keller-Miksis model, which includes the effects of acoustic radiation by treating the liquid as slightly compressible, was regarded slightly superior to other models based on Prosperetti and Lezzi's comparisons [38]; it is expressed by [38,52]

$$\left(1-c_\infty^{-1}\frac{dR}{dt}\right)R\frac{d^2R}{dt^2}+\frac{3}{2}\left(1-\frac{1}{3}c_\infty^{-1}\frac{dR}{dt}\right)\left(\frac{dR}{dt}\right)^2 = \left(1+c_\infty^{-1}\frac{dR}{dt}\right)\frac{1}{\rho_\infty}\left[p_B(t)-p_\infty-p_a\left(t+\frac{R}{c_\infty}\right)\right] + \frac{R}{\rho_\infty c_\infty}\frac{dp_B(t)}{dt}. \tag{19}$$

In Eq. (19), $p_B(t)$ is the pressure at the bubble wall; it is assumed to behave adiabatically, i.e., $p_B(t)=p_{B,0}(V_0/V)^\gamma$, where $p_{B,0}$ and V_0 are the initial pressure and the initial volume with V_0 corresponding to the initial bubble radius R_0 ($V_0=4\pi R_0^3/3$), and γ is the ratio of specific heats. For the small bubbles induced by the spark and the laser, we assumed $p_{B,0}/p_\infty=100$, $R_0/R_m=0.1485$, and $\gamma=1.25$ as suggested in Refs. [1,30] with the corresponding maximum radius R_m taken from Tables I and II. For the large underwater explosion bubbles, the initial pressure $p_{B,0}$ and the initial radius R_0 were determined as suggested in Refs. [1,41]: $p_{B,0}=1.39\times 10^5(W/V_0)^\lambda$, $\varepsilon/(\lambda-1)(R_0'^{3\lambda}-R_0'^3)=-1+R_0'^3$, $\varepsilon=p_{B,0}/p_\infty$, $R_0'=R_0/R_m$, and $\gamma=1.25$, with the corresponding charge weight W and the corresponding maximum radius R_m taken from Table III. In Eq. (19), p_a denotes the variable part of the pressure in the liquid at the location of the bubble

TABLE II. The measured data for the laser-generated bubbles; the predicted density parameter μ_L and the internal pressures with $p_\infty=0.1$ MPa, $\rho_\infty=1000$ kg/m^3, and $g=9.81$ m/s^2; EL stands for the index of energy level used in laser test.

External source	EL	D_L (m)	$(R_m)_L$ (mm)	$(t_c)_L$ (μs)	p_{max} (MPa)	μ_L [Eq. (12)]	P_i [Eq. (10)] (MPa)
Laser	18	0.03	0.599	62.0			
	20	0.03	0.649	67.2			
	24	0.03	0.729	75.4	<20	~ 0	0.022
	30	0.03	0.851	88.0			

TABLE III. The measured data for the bubbles generated by explosive charges of TNT and Hexocire [40,41], and the predicted density parameter μ_u and the internal pressures with $p_\infty=0.1$ MPa, $\rho_\infty=1000$ kg/m^3, and $g=9.81$ m/s^2.

External source	W (g)	D_u (m)	$(R_m)_u$ (m)	$(t_c)_u$ (ms)	p_{max} (MPa)	μ_u [Eq. (12)]	P_i [Eq. (10)]
TNT	300	91.5	0.482	15.0	203	0.074	~0
Hexocire	55	3.5	0.56	47.0	169	0.063	
	35	3.5	0.49	41.5	156	0.059	~0
	10	3.5	0.33	27.2	116	0.046	

center in the absence of the bubble [38], which is substituted with the hydrostatic pressure $\rho_\infty g D_\alpha$ with the corresponding water depth D_α taken from Tables I–III for the following comparison study. The sound speed, the density, and the pressure in the undisturbed fluid in Eq. (19) were assumed to be $\rho_\infty=1000$ kg/m^3, $p_\infty=0.1$ MPa, and $c_\infty=1500$ m/s for all the numerical simulations using the Keller-Miksis model.

Figure 5 compares the results among the Rayleigh model, the Keller-Miksis model, the present modified Rayleigh model, and the experimental data, respectively, for the spark and laser bubbles. Each radius-time curve in Fig. 5 was plotted from the time when the bubble radius reaches its maximum to the time at its collapse. The solid lines in Fig. 5 show the numerical results using the modified Rayleigh model [Eq. (5)], in which the data for the spark bubble (46 EL) in Table I and the data for the laser bubble (20 EL) in Table II were used. Note that $\mu_s\approx 0$, $p_i=0.3$ MPa for the spark bubble and $\mu_L\approx 0$, $p_i=0.22$ MPa for the laser bubble. The values of the maximum radii used in both the modified Rayleigh model and the Keller-Miksis model are the same, and they were taken from Tables I and II: $R_m=2.69$ mm for the spark bubble (46 V) and $R_m=0.649$ mm for the laser bubble (20 EL). Figure 5 shows that the results from both the Keller-Miksis model and the modified Rayleigh model [Eq. (5)] are much closer to experimental data than those from the Rayleigh model. This is due to fact that the retarding effect from the internal pressure is considered in these two models but is excluded in the Rayleigh model that simulates an empty bubble. Since we used $\mu_s\approx 0$ and $\mu_L\approx 0$ (i.e., $\Delta\rho_c\rightarrow 0$) for the spark and laser bubbles, the fact that the results from the modified Rayleigh model [Eq. (5)] matches the experimental data implies that the effect of the fluid compressibility on the small spark bubble and the small laser bubble is insignificant.

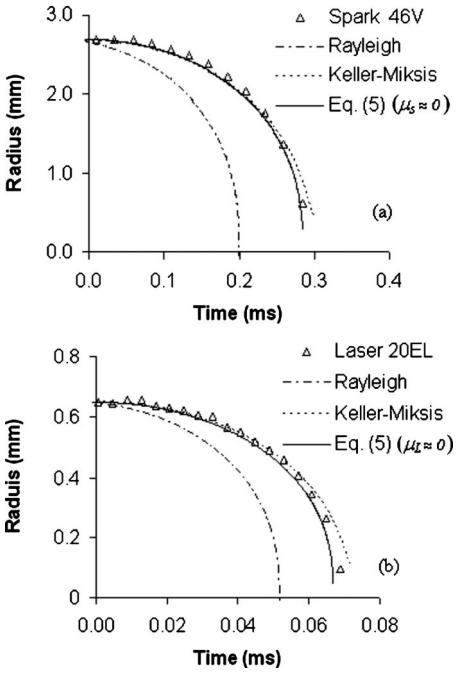

FIG. 5. Experimental bubble collapse vs numerical bubble collapse. (a) Comparison of the bubble induced by the spark (triangles) and the bubbles calculated with the Rayleigh model (dashed-dotted line), the Keller-Miksis model (dotted line), and Eq. (5) (solid line). (b) Comparison of the bubble induced by the laser (triangles) and the bubbles calculated with the Rayleigh model (dashed-dotted line), the Keller-Miksis model (dotted line), and Eq. (5) (solid line).

Figure 6 compares the results among the Rayleigh model, the Keller-Miksis model, the present modified Rayleigh model, and the experimental data for the bubbles induced, respectively, by the TNT and Hexocire explosions. Each radius-time curve in Fig. 6 was also plotted from the time when the bubble radius reaches its maximum to the time at its collapse. The solid lines in Fig. 6 show the radius-time curves using the modified Rayleigh model [Eq. (5)], in which $\mu_u=0.074$ for the bubble induced by the TNT charge of 300 g and $\mu_u=0.063$ for the bubble induced by the Hexocire charge of 55 g as shown in Table III. The dash lines in Fig. 6 show the radius-time curves which were also calculated using the modified Rayleigh model [Eq. (5)] but letting $\mu_u=0$, (i.e., $\Delta\rho_c=0$ for incompressible fluid) to examine the influence of the incompressibility assumption on the large underwater explosion bubbles. The significant difference between those results (dash line) with the incompressibility assumption ($\mu_u=0$) and the experimental data (triangles) shows that the influence of the fluid compressibility cannot be ignored when the maximum pressure at the fluid surrounding the bubble exceeds thousands of p_∞ (see Table III).

From Fig. 6, a slight difference is observed between the results from the Keller-Miksis model and the experimental data, which might be explained by the fact that the wave equation used in the Keller-Miksis model to accommodate the compressibility of the fluid is mainly accurate in the far field ($r\approx 2t_c c_\infty$) [38]. Figure 6 also shows that the results

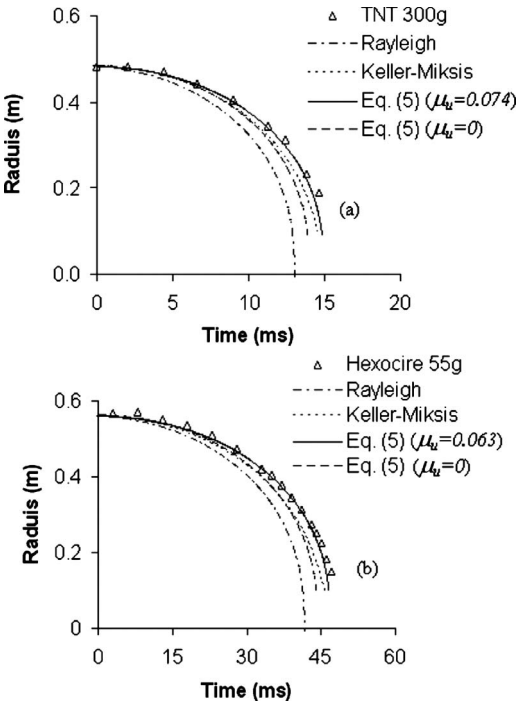

FIG. 6. Experimental bubble collapse vs numerical bubble collapse. (a) Comparison of the bubble induced by the underwater explosion of a TNT charge (triangles) and the bubbles calculated with the Rayleigh model (dashed-dotted line), the Keller-Miksis model (dotted line), Eq. (5) with μ_u=0.074 (solid line), and Eq. (5) with μ_u=0 (dashed line). (b) Comparison of the bubble induced by the underwater explosion of a Hexocire charge (triangles) and the bubbles calculated with the Rayleigh model (dashed-dotted line), the Keller-Miksis model (dotted line), Eq. (5) with μ_u=0.063 (solid line), and Eq. (5) with μ_u=0 (dashed line).

from the modified Rayleigh model [Eq. (5)], with μ_u =0.074 for the TNT bubble and μ_u=0.063 for the Hexocire bubble are closer to the experimental data. This is attributed to the density parameter μ_u which accommodates the effect of the compressed fluid with a high pressure surrounding the bubble wall at the collapse time. These results demonstrate that the present modified Rayleigh model provides a realistic simulation of bubble collapsing, and the density parameter μ_α is useful in accommodating the compressibility of the fluid with a high pressure at bubble collapse.

C. R_m and t_c of different bubbles

The maximum radius $(R_m)_u$ and the collapse time $(t_c)_u$ of a bubble generated by an explosive charge in deep water can be estimated using the empirical equations (14) and (5). In terms of the scaling relations (17) and (18), the maximum radius $(R_m)_u$ and the collapse time $(t_c)_u$ induced by the underwater explosion can also be represented by the maximum radius $(R_m)_\alpha$ and the collapse time $(t_c)_\alpha$ of a bubble induced by spark or laser.

Figure 7 shows the scaled maximum radius $(R_m)_\alpha$ and the collapse time $(t_c)_\alpha$ induced by the spark or the laser versus the maximum radius $(R_m)_u$ and the collapse time $(t_c)_u$ induced by the underwater explosion. The maximum radii and

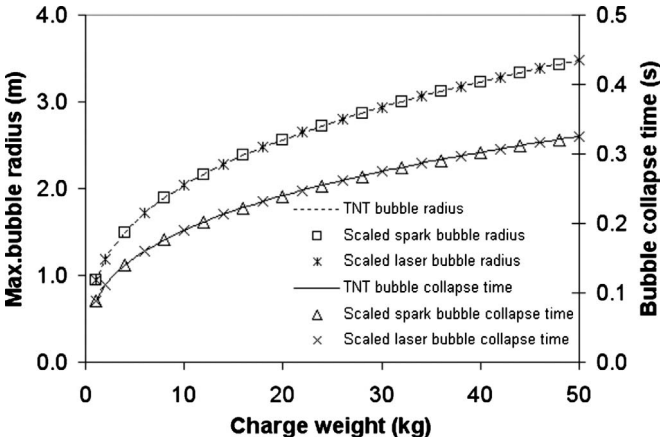

FIG. 7. Comparison of the maximum radii and the collapse times between underwater explosion bubbles with those of scaled spark- and laser-generated bubbles. The underwater explosion bubbles induced by TNT charges with various weights varying from 1 to 50 kg, detonated at the water depth of 35 m (D_u=35 m).

the bubble collapse times for the bubbles generated by TNT charges detonated at a water depth of 35 m were calculated using the empirical equations (14) and (15) with the charge weights varying from 1 to 50 kg. The constants for the TNT charge are K_R=3.36 $m^{4/3}$ $kg^{-1/3}$ and K_T=2.11 s $m^{5/6}$ $kg^{-1/3}$, which were taken from Ref. [40]. We may use the values $p_i \approx 0$ and μ_u=0.0748 in Table III which can also be determined by $\mu_u=[(K_T/K_R)(\sqrt{g}/1.83)-1]$ while ignoring the internal pressure in the collapse phase.

In consideration of the similarity in the spark- and laser-generated bubbles, we demonstrate with one set of spark-generated bubbles (46 V) and one set of laser-generated bubbles (23 EL) versus the underwater explosion bubbles in Fig. 7. By using Eqs. (17) and (18), the maximum radius $(R_m)_\alpha$ and the collapse time $(t_c)_\alpha$ induced by the spark (46 V) or the laser (23 EL) were scaled with the values of $p_i \approx p_v$ =0.3 MPa and $\mu_s \approx 0$ in Table I for the spark-generated bubble, and the values of $p_i \approx 0.22$ MPa and $\mu_L \approx 0$ in Table II for the laser-generated bubble. Figure 7 shows that both the scaled maximum radius and the scaled collapse time of the spark- or laser-generated bubbles match well with the bubbles induced by TNT explosive charges with various weights at deep water. These results illustrate that R_m and t_c of the spark- and laser-generated bubbles can be used to represent R_m and t_c of the underwater explosion bubbles via the scaling relations (17) and (18).

D. Dimensionless R'-t' curves for different bubbles

The dimensionless bubble radius as a function of dimensionless time in the collapse phase can be calculated by integrating numerically Eq. (8), which implies that the actual (dimensional) R-t curves of different bubbles in their collapse phase can be unified. Furthermore, the dimensionless R'-t' curve can be extended to approximate the variation of the dimensionless bubble radius with dimensionless time in the growth phase, by plotting the dimensionless R'-t' curve in the growth phase symmetrically about the point of the maximum radius as suggested in Refs. [8,18].

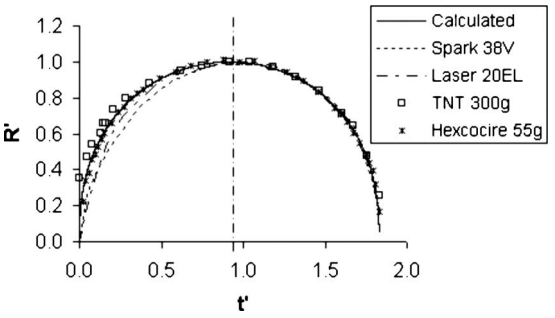

FIG. 8. The dimensionless R'-t' curves of the bubbles, respectively, nondimensionalized from the bubbles generated by the spark, the laser, and the underwater explosions as well as the curve calculated by integrating numerically Eq. (8).

Figure 8 shows the dimensionless R'-t' curves of the nondimensionalized bubbles generated by the spark, the laser, and the underwater explosions, respectively, as well as the dimensionless R'-t' curve calculated by integrating Eq. (8) numerically. The calculated R'-t' curve fits well with the R'-t' curves nondimensionalized from the different measured bubbles in the collapse phase ($0.915 \leq t' < 1.83$). This implies that the different bubbles induced by different external sources can be described by the modified Rayleigh model in their collapse phases.

A small difference between the calculated R'-t' curve and the measured R'-t' curves in the bubble growth phase ($0 < t' < 0.915$) is observed in Fig. 8, which shows that the modified Rayleigh model is not quite adequate to accurately describe the different bubbles at their early stage. This may be explained that at their early stage, the energy conversion of different external sources may be accompanied by very complex physical phenomena such as high temperature, high pressure, high compressibility of fluid, and shock wave propagation with high Mach number, etc. For example, in the underwater explosion [39], the released energy at the instant following the detonation is present in the form of potential energy with exceedingly high pressure and temperature in the resulting volume of gas. As the initial underwater explosion bubble proceeds to expand, it transfers energy to the water, and part of this energy is gradually dissipated by conversion into thermal energy which elevates the temperature of the surrounding fluid through which the pressure wave is propagated. The remaining energy, which is transferred to the water, is imparted as kinetic energy [39]. The bubble expansion continues as the water is being pushed radially outward against the opposing hydrostatic pressure, until the energy available to this phase of the motion is stored as potential energy in the water. (It is noted that the reader can refer to more comprehensive theories described in previous works [4,38,42,43,46–53] which can possibly be further developed, so that the very complex physical phenomena such as high pressure, highly compressed fluid, high temperature, etc. during the bubble expansion are accounted for. This is outside the scope of the current work.)

With inspecting the R'-t' curves shown in Fig. 8, it follows that the modified Rayleigh model is reasonable in describing the different bubbles in their collapse phase. It is, however, not quite adequate to describe quantitatively the initial stage of bubble expanding. Nevertheless, it retains the simplicity and feasibility if only a qualitative analysis or description of the bubble expansion is desired in certain practical applications; for example, in the study of underwater explosion, the interest lies in the contraction and collapse of the bubble rather than its expansion phase since serious damage to the nearby structures is most likely due to the contraction and collapse of the bubble induced by an underwater explosion.

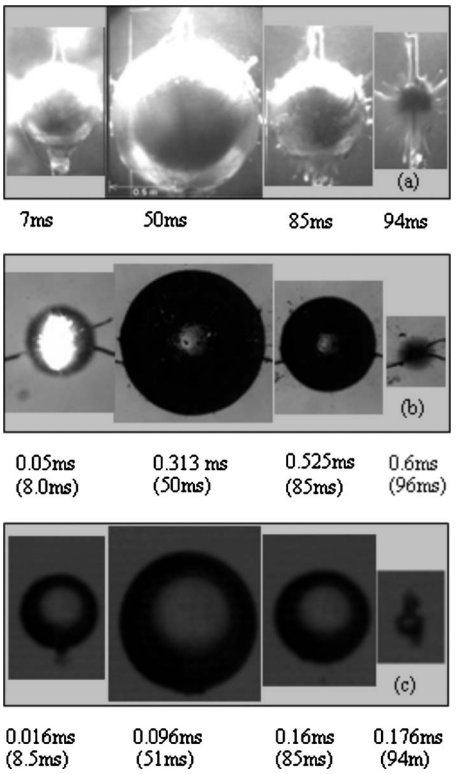

FIG. 9. Comparison of the images of a measured underwater explosion bubble with measured spark- and laser-generated bubbles. (a) The measured underwater explosion bubble induced by a 55 g Hexocire explosive charge detonated at a depth of 3.5 m, at 7, 50, 85, and 94 ms. (b) The measured spark-generated bubble (46 V) at 0.05, 0.313, 0.523, and 0.6 ms, and their corresponding scaled time instants in the brackets: 8.0, 50, 86, and 96 ms with $\lambda_R = 209$, $\lambda_T = 161$. (c) The measured laser-generated bubble (30 EL) at 0.016, 0.096, 0.16, and 0.176 ms, and their corresponding scaled time instants in the brackets: 8.5, 51, 85, and 94 ms with $\lambda_R = 658$, $\lambda_T = 534$.

E. Substitution of a spark- or laser-generated bubble for an underwater explosion bubble

Based on Eqs. (17) and (18), the dimensional R-t curve of an underwater explosion bubble in the collapse phase can be represented by the dimensional R-t curve of a spark- or laser-generated bubble. Figure 9(a) displays four images of the

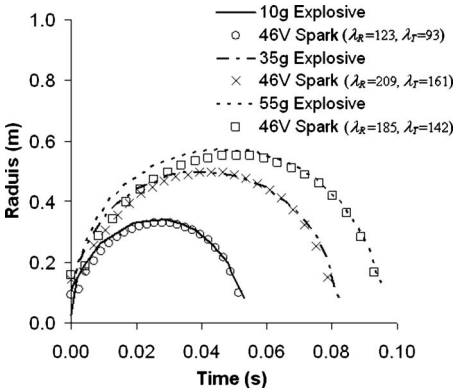

FIG. 10. Comparison of the spark-generated bubble (46 V), which was scaled using Eqs. (17) and (18), with the bubbles generated, respectively, by Hexocire explosive charges of 10, 35, and 55 g at a water depth of 3.5 m.

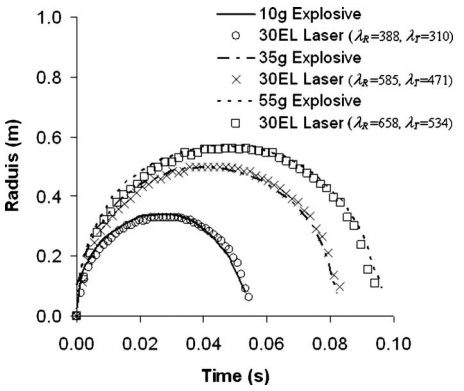

FIG. 11. Comparison of the laser-generated bubble (30 EL), which was scaled using Eqs. (17) and (18), with the bubbles generated, respectively, by Hexocire explosive charges of 10, 35, and 55 g at a water depth of 3.5 m.

same bubble created by the explosive charge of Hexocire (RDX+wax) with a weight of 55 g detonated at a depth of 3.5 m [41]. The measured time instants for the four images of the underwater explosion bubble are 7, 50, 85, and 94 ms with respect to the moment of detonation. The underwater explosion bubble grows to its maximum radius of 560 mm at $t=50$ ms.

Figure 9(b) shows the measured images of the spark-generated bubble (46 V) at four time instants of 0.05, 0.313, 0.525, and 0.6 ms while Fig. 9(c) depicts the measured images of the laser-generated bubble (30 EL) at four time instants of 0.016, 0.096, 0.16, and 0.176 ms. We scale the spark-generated bubble with the length scale factor of $\lambda_R=209$ and the time scale factor of $\lambda_T=161$, and scale the laser-generated bubble with the length scale factor of $\lambda_R=658$ and the time scale factor of $\lambda_T=534$ using Eqs. (17) and (18). The scaled time instants for the spark-generated bubble (46 V) become 8, 50, 85, and 96 ms [shown in brackets in Fig. 9(b)], respectively, with the scaled maximum radius of 560 mm occurring at about the scaled time of 50 ms. The scaled time instants for the laser-generated bubble (30 EL) become 8.5, 51, 85, and 94 ms [shown in brackets in Fig. 9(c)], respectively, with the scaled maximum radius of 560 mm occurring at about the scaled time of 51 ms. Both the scaled spark- and laser-generated bubbles concur well with the corresponding time instants and maximum radius for the underwater explosion bubble.

Next, we scale the spark- or laser-generated bubbles to match the various underwater explosion bubbles, generated by three different charge weights of 10, 35, and 55 g at a depth of 3.5 m [41]. In consideration of similarity in the scaled spark- and laser-generated bubbles as shown in Fig. 3, we plot the results for comparison of one data set (46 V) of the scaled spark-generated bubble with the measured underwater explosion bubbles as shown in Fig. 10. Separately, the corresponding results for the comparison of one data set (30 EL) of the scaled laser-generated bubble with the measured underwater explosion bubbles are shown in Fig. 11.

Figure 10 shows that the scaled spark-generated bubble radius is slightly smaller than the measured underwater explosion bubble radius in the earlier time when the bubble is expanding for all cases. In the collapse phase, however, all the scaled spark-generated bubbles match well with the measured underwater explosion bubbles. Figure 11 shows that the radius of the scaled laser-generated bubbles matches all the measured underwater explosion bubbles in the whole process of bubble expansion, contraction, and collapse. Overall, these results indicate that the present scaling law is effective for using spark- or laser-generated bubbles to represent underwater explosion bubbles.

V. CONCLUSION

We have presented the scaling law based on the modified Rayleigh model for the bubbles induced by different external sources. The density parameter μ_α that accommodates the compressibility of the fluid surrounding a collapsing bubble was incorporated in the modified Rayleigh model. It has been shown useful in establishing the scaling relationship between different bubbles on which the density change exhibits different effects. With the present scaling law, the spark- and laser-generated bubbles can be scaled to simulate underwater explosion bubbles induced by explosive charges with different weights at different water depths. This enables the possible substitution of experiment of underwater explosion with a spark- or laser-generated bubble for future investigation of explosion bubble behaviors (for example, an explosion bubble near some complex structures where the dynamics of the bubble can be studied). This substitution is practical and may be necessitated by the desire to avoid environmental pollutions, and for reducing cost of experimentation. On the other hand, with the present scaling law the experiences built up over the years in underwater explosion bubbles could be explored for the spark- and laser-generated bubbles in biomedical related applications, such as LASIK and laser glaucoma treatment.

ACKNOWLEDGMENTS

We thank National University of Singapore's Impact Mechanics Laboratory for their help and support for the spark-generated bubble test. Also, we thank the Nanyang Technological University's Cavitation Laboratory for their support on the laser generation bubble experiment. In addition, we would like to thank the referees for their helpful comments and suggestions.

[1] R. H. Cole, *Underwater Explosions* (Princeton University Press, Princeton, NJ, 1948).
[2] J. R. Blake and D. C. Gibson, Annu. Rev. Fluid Mech. **19**, 99 (1987).
[3] W. Lauterborn, Appl. Phys. Lett. **21**, 27 (1972).
[4] T. L. Geers and K. S. Hunter, J. Acoust. Soc. Am. **111**, 1584 (2002).
[5] Y. Tomita and A. Shima, J. Fluid Mech. **169**, 535 (1986).
[6] G. L. Chahine, G. S. Frederick, C. J. Lambrecht, G. S. Harris, and H. U. Mair, Proceedings of the 66th Shock and Vibration Symposium, Biloxi, MS (1995), p. 265.
[7] J. A. Cook, A. M. Gleeson, R. M. Roberts, and R. L. Rogers, J. Acoust. Soc. Am. **101**, 1908 (1997).
[8] S. Buogo and G. B. Cannelli, J. Acoust. Soc. Am. **111**, 2594 (2002).
[9] J. R. Krieger and G. L. Chahine, J. Acoust. Soc. Am. **118**, 2961 (2005).
[10] D. Obreschkow, P. Kobel, N. Dorsaz, A. deBosset, C. Nicollier, and M. Farhat, Phys. Rev. Lett. **97**, 094502 (2006).
[11] I. Akhatov, O. Lindau, A. Topolnikov, R. Mettin, N. Vakhitova, and W. Lauterborn, Phys. Fluids **13**, 2805 (2001).
[12] P. B. Robinson, J. R. Blake, T. Kodama, A. Shima, and Y. Tomita, J. Appl. Phys. **89**, 8225 (2001).
[13] E. A. Brujan, K. Nahen, P. Schmidt, and A. Vogel, J. Fluid Mech. **433**, 251 (2001).
[14] E. A. Brujan, K. Nahen, P. Schmidt, and A. Vogel, J. Fluid Mech. **433**, 283 (2001).
[15] Y. Tomita and T. Kodama, J. Appl. Phys. **94**, 2809 (2003).
[16] G. N. Sankin, W. N. Simmons, S. L. Zhu, and P. Zhong, Phys. Rev. Lett. **95**, 034501 (2005).
[17] E. Zwaan, S. Le Gac, K. Tsuji, and C. D. Ohl, Phys. Rev. Lett. **98**, 254501 (2007).
[18] R. Petkovšek and P. Gregorčič, J. Appl. Phys. **102**, 044909 (2007).
[19] P. Gregorčič, R. Petkovšek, and J. Možina, J. Appl. Phys. **102**, 094904 (2007).
[20] C. E. Brennen, *Cavitation and Bubble Dynamics* (Oxford University Press, New York, 1995).
[21] C. D. Ohl and R. Ikink, Phys. Rev. Lett. **90**, 214502 (2003).
[22] W. D. Song, M. H. Hing, B. Lukyanchuk, and T. C. Chong, J. Appl. Phys. **95**, 2952 (2004).
[23] P. Marmottant and S. Hilgenfeldt, Nature (London) **423**, 153 (2003).
[24] E. Klaseboer and B. C. Khoo, J. Appl. Phys. **96**, 5808 (2004).
[25] C. K. Turangan, G. P. Ong, E. Klaseboer, and B. C. Khoo, J. Appl. Phys. **100**, 054910 (2006).
[26] E. Sassaroli and K. Hynynen, Appl. Phys. Lett. **89**, 123901 (2006).
[27] S. W. Gong and K. Y. Lam, Int. J. Impact Eng. **32**, 1857 (2006).
[28] M. Ida, T. Naoe, and M. Futakawa, Phys. Rev. E **75**, 046304 (2007).
[29] M. Ida, T. Naoe, and M. Futakawa, Phys. Rev. E **76**, 046309 (2007).
[30] E. Klaseboer, S. W. Ohl, C. K. Turangan, B. C. Khoo, A. J. Szeri, M. Calvisi, G. N. Sankin, and P. Zhong, J. Fluid Mech. **593**, 33 (2007).
[31] J. Holzfuss, Phys. Rev. E **78**, 025303(R) (2008).
[32] O. Louisnard, Phys. Rev. E **78**, 036322 (2008).
[33] M. Ida, Phys. Rev. E **79**, 016307 (2009).
[34] L. E. Probst, *LASIK: Advances, Controversies, and Custom* (SLACK Incorporated, New Jersey, 2004).
[35] S. W. Ohl, E. Klaseboer, and B. C. Khoo, Phys. Med. Biol. **54**, 6313 (2009).
[36] L. Rayleigh, Philos. Mag. **34**, 94 (1917).
[37] A. Pearson, J. R. Blake, and S. R. Otto, J. Eng. Math. **48**, 391 (2004).
[38] A. Prosperetti and A. Lezzi, J. Fluid Mech. **168**, 457 (1986).
[39] A. B. Arons and D. R. Yennie, Rev. Mod. Phys. **20**, 519 (1948).
[40] E. Swift and J. C. Decius, *Underwater Explosion Research* (Office of Naval Research, Washington, D.C., 1950), Vol. II.
[41] E. Klaseboer, K. C. Hung, C. Wang, C. W. Wang, B. C. Khoo, P. Boyce, S. Debono, and H. J. Charlier, J. Fluid Mech. **537**, 387 (2005).
[42] E. A. Neppiras, Phys. Rep. **61**, 159 (1980).
[43] F. R. Young, *Cavitation* (McGaw-Hill Book Company, New York, 1989).
[44] K. S. F. Lew, E. Klaseboer, and B. C. Khoo, Sens. Actuators, A **133**, 161 (2007).
[45] A. B. Arons, J. Acoust. Soc. Am. **20**, 277 (1948).
[46] C. Herring, Columbia University NDRC Report No. C-4-sr 10-010, 1941 (unpublished).
[47] L. Trilling, J. Appl. Phys. **23**, 14 (1952).
[48] F. R. Gilmore, California Institute of Technology Hydrodynamics Laboratory Report No. 26-4, 1952 (unpublished).
[49] R. Hickling and M. S. Plesset, Phys. Fluids **7**, 7 (1964).
[50] M. S. Plesset and A. Prosperetti, Annu. Rev. Fluid Mech. **9**, 145 (1977).
[51] A. Fujikawa and T. Akamatsu, J. Fluid Mech. **97**, 481 (1980).
[52] J. B. Keller and M. Miksis, J. Acoust. Soc. Am. **68**, 628 (1980).
[53] A. Prosperetti, J. Fluid Mech. **222**, 587 (1991).